Available online at www.sciencedirect.com
SCIENCE DIRECT
International Journal of Heat and Mass Transfer 49 (2006) 2009–2019
International Journal of HEAT and MASS TRANSFER
www.elsevier.com/locate/ijhmt

An experimental study of thermally induced convection of molten gallium in magnetic fields

B. Xu, B.Q. Li *, D.E. Stock

School of Mechanical and Materials Engineering, Washington State University, P.O. Box 642920, Pullman, WA 99164, United States

Received 10 March 2005; received in revised form 21 November 2005
Available online 9 March 2006

Abstract

This paper presents an experimental investigation on natural convection in a molten metal subject to a uniform magnetic field. The working fluid is molten gallium, which is contained in a rectangular box with the two opposite vertical walls held at different temperatures. The imposed magnetic fields are parallel to the temperature gradient. Both the temperature and velocity fields are measured with and without an imposed magnetic field. Numerical simulations of convective flows in the system are also performed using the numerical model developed in a previous study. Good agreement exists between the measured and computed results for the conditions studied. Results show that natural convection is suppressed with an imposed magnetic field and the magnetic damping effect increases with an increase in the applied field strength.

Keywords: Natural convection; Gallium; Hot-film anemometry

1. Introduction

Natural convection occurs in a thermal system where a temperature gradient exists. One such system is the melt growth of single crystals, in which thermally induced convection plays an important role in affecting the formation of defects such as dopant segregation or striation during the melt growth of these crystals [1]. The widespread use of the processes for electronic and optical applications has resulted in extensive research towards the understanding and hence control of natural convection in these systems.

One of the effective means practiced in industry for thermally induced melt flow control is magnetic damping, which is derived from the interaction between an electrically conducting melt flow and an applied magnetic field to generate an opposing Lorentz force to the convective flows in the melt. The damping effect depends on the strength of the applied magnetic field and its orientation with respect to the convective flow direction. Substantial theoretical and numerical work thus far has appeared on magnetic damping for natural convection [2–11]. Ozoe and Okada [4] conducted a numerical analysis of the magnetic damping effect in a cubic cavity with two vertical walls at different temperatures. They found that the strongest damping effect is achieved with the magnetic field applied perpendicular to the hot wall. This is consistent with the work of Alboussière et al. [5] who used an asymptotic approach, and found that for a rectangular box, the damping effect is the weakest when the applied magnetic field is horizontal and parallel to the hot wall. BenHadid and Henry [6] studied numerically the damping of steady flow induced by temperature gradients using a $4 \times 1 \times 1$ (length × width × height) cavity with the magnetic field applied in different directions. Their results are in good agreement with the analytical predictions from Alboussière et al. [5] and Garandet et al. [7]. Recent research on the subject has been on exploring the possibility of applying magnetic damping concept to control the g-jitter induced natural convection in microgravity environment [8–11].

* Corresponding author. Tel: +1 509 335 7386; fax: +1 509 335 4662.
E-mail address: li@mme.wsu.edu (B.Q. Li).

0017-9310/$ - see front matter © 2006 Published by Elsevier Ltd.
doi:10.1016/j.ijheatmasstransfer.2005.11.033

Despite the extensive analytic and numerical work, there appears to have been very limited experimental work on natural convection in a melt, in particular the direct measurement of convective flows in a thermal gradient. Much of the limited experimental work has been on the temperature measurements only. Among the earliest experimental investigations on the magnetic damping of the thermally induced natural convection are those by Hurle et al. [12,13]. They observed temperature oscillation in molten gallium contained in an open rectangular container. The oscillation is reduced when a magnetic field is applied perpendicular to the main convective flow. Okada and Ozoe [14] measured the temperature profile in the molten gallium contained in a cubic cavity. The measurements validated their numerical modeling results reported earlier [4]. Davoust et al. [15] experimentally studied, through thermal measurements, the effect of magnetic damping on a horizontal cylinder filled with mercury subjected to a vertical magnetic field. The data collected were used to verify the theoretical predictions of Alboussière et al. [16] and BenHadid and Henry [17]. Juel et al. [18] conducted a combined numerical and experimental investigation on magnetic damping of the temperature gradient induced natural convection. They measured vertical temperature difference in molten gallium contained in a rectangular channel with an applied horizontal temperature gradient. Their experimental and numerical results are in good agreement. They also found that with the increase of the Hartmann number, flow becomes 2-D. A similar experimental system was later used by Hof et al. [19] to measure the dependence of the damping effect on the orientation of the magnetic field.

All of the aforementioned experimental investigations have been on the temperature measurements from which magnetic damping effects are deduced. There seems to be little work, if not at all, on the direct measurement of thermally induced melt convection in the presence or absence of an external magnetic field. The need for these measured data cannot be over-emphasized. An experimental study of this type is of crucial importance in providing a database to directly validate the numerical predictions of convective flows from the numerical models in existence and under development. It should also be of great value in direct interpreting the physics governing the magnetic damping effects on convective flows in thermal processing systems.

This paper presents an experimental study of natural convection in molten gallium with and without an imposed magnetic field. The experimental system consists of a rectangular cell with a prescribed thermal gradient controlled by two thermal baths. The temperature is measured using the thermocouples and the melt flow velocity field is determined using the hot-wire probes. The measured velocity and temperature profiles are used to compare with the predictions from numerical models developed in early studies [11]. There exists good agreement between the numerical predictions and experimental measurements. Magnetic damping effects are observed in both the temperature and the velocity profiles when an external magnetic field is applied. The measured velocity and temperature fields should provide a valuable experimental database against which other numerical models developed for natural convection with and without an imposed magnetic field can be validated.

2. Experimental facility and instrumentation

2.1. Gallium

For the present study, molten gallium with a melting point of 302 K was used as the working fluid. Molten gallium is opaque and bright silver in color. Some of its thermal physical properties are listed in Table 1 along with the properties of two other liquid metals, mercury and liquid sodium [20,21], that are commonly used as working fluids to study heat transfer and convection in liquid metals. Gallium's electrical and thermal conductivities are about four times higher than that of mercury, which makes it an outstanding working fluid for MHD research. Compared with mercury and sodium, gallium is easier and safer to handle because of its low toxicity and low vapor pressure. The initial gallium sample used in the present experiments has a purity of 99.99%.

2.2. Testing cavity

The test cell used in our study was a rectangular container 3-cm deep by 3-cm wide by 15-cm long, which is shown in Fig. 1. The two long vertical walls were made of copper and attached to constant temperature water baths. The temperatures of the water baths were controlled within an accuracy of ± 0.05 K. A horizontal temperature gradient was applied across the gallium inside the cell by varying the temperatures of the water baths. The open top surface of the cell facilitated the traversing of the hot-film probe and the thermocouple. The other walls of the cell were made of 3-mm Plexiglas whose thermal conductivity is 0.2 W/(mK), about 1/150 that of the gallium. It was observed that a layer of the gallium covered and stayed on the copper walls shortly after the copper walls were in contact with the gallium. Visual observation reveals no further deterioration on the copper plates.

Table 1
Thermal physical properties of some liquid metals

Properties		Gallium	Mercury	Sodium
Density	kg/m^3	6.09×10^3	13.59×10^3	0.93×10^3
Kinematic viscosity	m^2/s	3.1×10^{-7}	1.14×10^{-7}	7.75×10^{-7}
Electric conductivity	$(m\Omega)^{-1}$	3.68×10^6	1.04×10^6	10.35×10^6
Thermal conductivity	W/(mK)	31	8.3	142
Melting point	°C	29	−39	98
Boiling point	°C	2227	356	881
Coefficient of thermal expansion	K^{-1}	1.27×10^{-4}		
Surface tension	N/m	0.735		

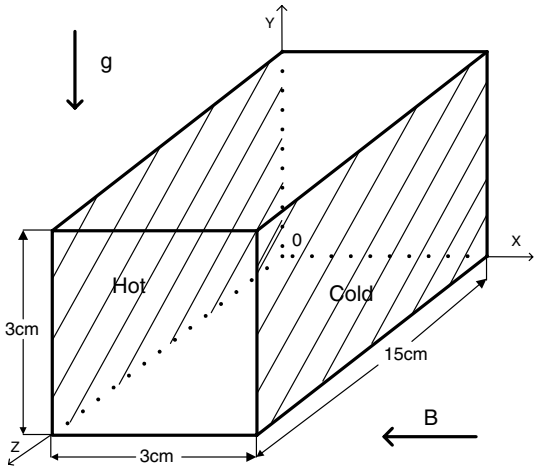

Fig. 1. Testing cell for the experimental study of thermally induced melt flows. Here O denotes the origin of the coordinate system.

2.3. Magnetic field

The cell containing the gallium was placed between two electromagnet poles, of 10 in. diameter, of a Walker Scientific Inc. (Model #: HV10H) (see Fig. 2(a)). A field strength of up to 10^4 Gauss over an air gap of 10 cm can be generated. A Walker Scientific Inc. HS-1785 DC power supply was used as the power source for the electromagnets. The power supply provides a stabilized current control, which ensures the stability of the magnetic fields. The strength of the magnetic field was controlled by regulating the DC power input to the coils around the electromagnets. In the present experiment, field strengths of 300 and 3500 Gauss, over an air gap of 20 cm were used, which corresponded to 15 Amp and 50 Amp DC input at 75 V, respectively. Spatial uniformity of the magnetic field was assessed by measuring the horizontal magnetic field using

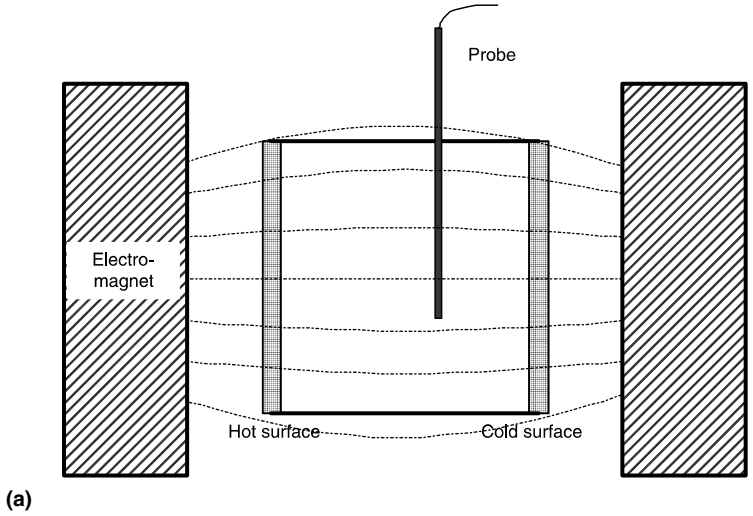

(a)

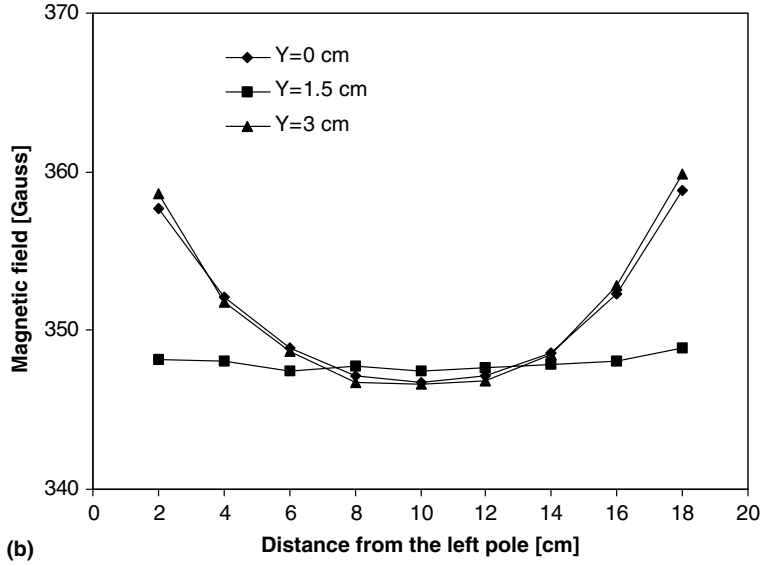

(b)

Fig. 2. (a) Placement of the experimental apparatus for the measurement of the temperature and velocity field distributions in molten gallium subject to applied magnetic fields. (b) Distribution of the horizontal magnetic field strengths along $Y = 0.0$ cm, 1.5 cm and 3.0 cm for air gap of 20 cm and 15 Amp DC power supply.

a S.W. Bell 9950 Gaussmeter. Typical magnetic field distributions within the cross-sectional plane at the middle of the Z-direction are shown in Fig. 2(b). Considering the size of the testing cell, the spatial variation of the magnetic field strength is less than 0.5%.

2.4. Hot-film probe

A standard TSI 1210 cylindrical single sensor hot-film probe was used with a TSI 1050 anemometer working in the constant temperature mode with an over-heat ratio of 1.1 for a fluid temperature of 341 K. This relatively high over-heat ratio value was used to reduce the temperature sensitivity at low velocities [24]. The bridge voltage was measured with an HP 3478A voltmeter.

The probe was 1 mm long with an aspect ratio of approximately 20. The probe was coated with a 2 μm layer of quartz to insulate it from the gallium. The diameter of the probe is small compared with the size of the container. Hence the influence of the presence of the probe on the natural convection was negligible. At very low velocities, the flow around a hot-film anemometer probe is a combination of the externally imposed flow and the natural convection due to the temperature difference between the probe and the surrounding fluid [31]. Generally, the effects of the natural convection induced by the probe can be neglected if the cubic root of the Grashof number for the probe is less than the Reynolds number based on the probe diameter [30]. For our experiment, the sensor outer diameter was 50 μm, temperature difference between the probe and the gallium was 15 K, and typical velocity was 1 cm/s, which give a Reynolds number of 1.6, and a Grashof number of 0.025. Therefore, the effect of probe induced natural convection can be neglected except for velocities below 0.2 cm/s. At the low velocities the magnetic field could alter the probe induced natural convection flow and therefore the heat transfer from the probe [27–29]. Since the purpose of the work is to investigate the effect of a magnetic field on natural convection, it is difficult to predict *a priori* when this effect will be important. However, as long as the probe induced natural convection is not important it can be assumed the magnetic field will not affect the hot-film probe. Lykoudis and Dunn [29] calibrated hot-film probes in mercury over a Reynolds number range of 0–130 and Hartmann number range from 0 to 4.68. They found that the cubic root criterion suggested by Collis and Williams [30] predicts the critical Reynolds number between the free and forced convection regions well. In present experiment, the Hartmann number was 0.78 when the applied magnetic field strength was 3500 Gauss. The effect of the magnetic field on the probe can be ignored in the present study.

The hot-film probe was calibrated using a rotating platform consisting of an inner container, which held the gallium, and an outer water jacket. The system is sketched in Fig. 3. The temperature of the gallium was regulated by running hot water from a constant temperature water bath through the water jacket. The outer wall of the water jacket was made hollow and filled with water (shaded in Fig. 3). The large volume and high heat capacitance of the water helped to minimize a temperature drift with ± 0.05 K during the calibration. A variable speed motor capable of an angular velocity of 20–65 rpm was used to rotate the double container to generate the tangential flow needed for calibration. A type T thermocouple, an ice bath, and an HP 33420A nano-voltmeter were used to measure the temperature of the gallium at the same radial position that was used to calibrate the hot-film probe.

Using a hot-film probe in liquid metals is plagued by the problem of random bridge output offset caused by a layer of impurities that form at the interface between the liquid metal and the probe surface when the probe is immersed into the liquid metal. The impurity layer creates a contact thermal resistance that changes the heat transfer rate between the probe and the liquid metal. The thickness of the impurity layer changes each time the probe is re-immersed into the liquid gallium. This results in a non-predictable offset in anemometer bridge output. Sajben [22] proposed that the effects of the impurity layer can be eliminated by using an $X(Pe)$ function, given by

$$X(Pe) = \pi k_f L_p \Delta T \left(\frac{1}{Q(0)} - \frac{1}{Q(Pe)} \right), \tag{1}$$

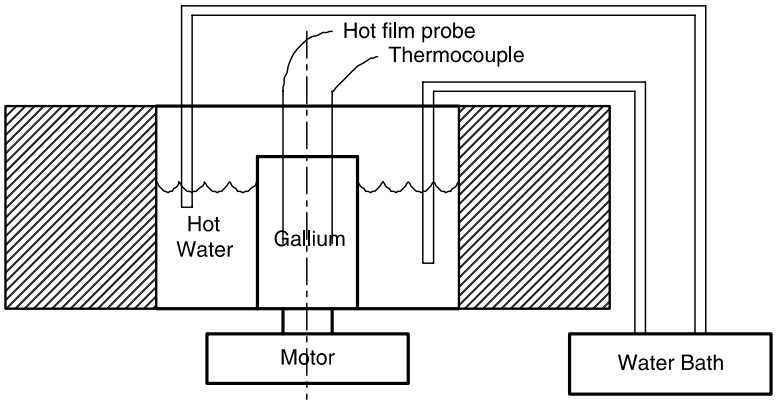

Fig. 3. The turntable facility for calibration of the hot-wire probe used in the present study.

where k_f is the thermal conductivity of the liquid, L_p the length of the hot-film probe, and ΔT the temperature difference between the probe and the liquid. $Q(0)$ and $Q(Pe)$ are heat transfer rates at a flow velocity of zero and at test conditions, respectively. Pe is the Péclet number, which, for a given temperature, is a non-dimensional velocity given by

$$Pe = \frac{Ud}{\alpha}, \tag{2}$$

where U is the velocity, and d the outer diameter of the hot-film probe. At steady state, the heat dissipation rate from the hot-film probe can be determined from the anemometer bridge output by

$$Q = \frac{E^2 R_P}{(R_P + R_T)^2}, \tag{3}$$

where E is the bridge output from the anemometer, R_P the resistance of the hot-film probe, and R_T the resistance in series with R_P. R_T is a combined resistance of the leads and the probe holder body, which was measured by a multimeter with the probe replaced by a jumper wire. The combined resistances of R_P and R_T were measured using the resistance decades in the anemometry and then R_P was determined by subtracting R_T from the measured resistance. The values of the resistances are listed in Table 2.

ΔT was determined using the operating temperature of the hot-film probe, calculated using an over-heat ratio of 1.1 and the temperature coefficient of resistance of the probe, and the temperature of the molten gallium, which was measured using a thermocouple. Ignoring the temperature dependence of fluid properties, combining Eqs. (1) and (3) gives

$$X(Pe) = \frac{\pi k_f L \Delta T (R_P + R_T)^2}{R_P} \left(\frac{1}{E^2(0)} - \frac{1}{E^2(Pe)} \right). \tag{4}$$

We observed that in addition to the constant offset of the bridge voltage due to impurities, the bridge output varied continuously with time. This continuous drifting of signal was probably caused by an unknown chemical reaction between the liquid gallium and the impurities coating of the hot-film probe. The continuous drifting decreased to an acceptable level after the probe had been immersed in the gallium for several hours; therefore the probe was aged in the liquid gallium, with the probe hot, for at least 4 h before being used.

Table 2
Calibration constants

T (K)	328	333	339	341
A_0	5.68×10^{-2}	1.14×10^{-1}	1.35×10^{-1}	4.27×10^{-3}
A_1	3.26×10^{3}	4.00×10^{3}	6.46×10^{3}	1.85×10^{4}
A_2	-8.51×10^{5}	-1.30×10^{6}	-3.41×10^{6}	-3.26×10^{7}
B_0	1.73×10^{1}			
B_1	2.40×10^{-2}			
B_2	-3.96×10^{-5}			
R_P	8.03 Ω			
R_T	0.20 Ω			

The anemometer bridge voltage is a function of both the velocity and the temperature of the gallium. Because the flow being studied was natural convection and therefore both the velocity and temperature varied through the container, the probe had to be calibrated over the full range of temperatures and velocities that might occur in the experiment. Various temperature compensation schemes are available [25,26], but they all require that the temperatures of the fluid and the probe be determined with very low bias error. In this experiment, because only a few measurements were required, the uncertainty was minimized by calibrating the probe over the full temperature and velocity ranges and building a lookup relationship for each measurement. The calibration was done at four constant temperatures, 328 K, 333 K, 339 K and 341 K, and for velocities between 0.5 and 2.8 cm/s at each temperature. During the calibration process, the bridge output was recorded at no-flow condition and then over the velocity range at each temperature setting. This process was repeated for each of the four temperatures. The measured bridge outputs were converted to $X(Pe)$ using Eq. (7) for each temperature. The $X(Pe)$-velocity data for each of the four temperatures were curve-fit using

$$U = A_0 + A_1 X(Pe) + A_2 X(Pe)^2, \tag{5}$$

where U is the velocity, Fig. 4. Typical values for the constants in Eq. (5) are given in Table 2. The shape of the curves shown in Fig. 4 resembles that found by Malcolm [23]. Because the over-heat ratio increases as the fluid temperature decreases, the probe is more sensitive at lower fluid temperatures. The calibration was reproducible from one experiment to another over two months within ±10%. Measured calibration velocities have an uncertainty of ±0.2 cm/s and temperatures have a bias uncertainty of ±0.5 K.

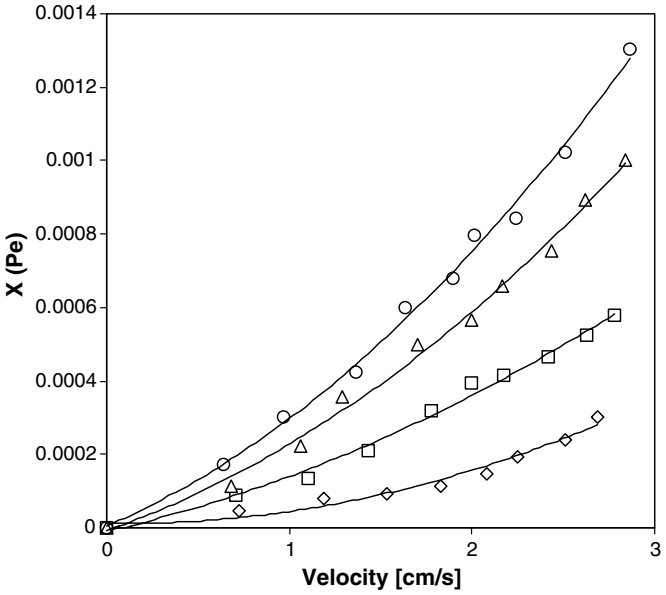

Fig. 4. Calibration curves for the constant temperature hot-wire probe at different temperatures: circles 328.15 K, triangle 333.15 K, squares 339.15 K and diamonds 341.15 K.

Most liquid metals react with the oxygen in air. Conventionally, the surface of liquid metals is covered with a thin layer of water to stop this reaction. We found that keeping a layer of water on the top of open liquid gallium surface introduced unwanted disturbance to the temperature field, therefore no water was placed on top of the gallium surface. We did observe that after exposing the free surface of the gallium to air for several minutes, a layer of gallium oxide formed. This layer of oxide insulated the gallium from direct contact with ambient air. After each set of measurements, the oxide and scum were removed from the gallium to keep the gallium clean. No residue was found at the bottom of the cell after the experiments. The probe itself was not cleaned during the experiments.

2.5. Measurements

Measurements were taken within cross-sectional surface of $Z = 7.5$ cm at vertical locations of $Y = 0.25$ cm, 1.5 cm and 2.75 cm and in increment of 0.25 cm in the X direction at each vertical level. The probe was accurately positioned in the gallium using a screw-driven manipulator affixed to the electromagnet. Each time the probe was inserted into the gallium it was allowed to stabilize for at least 4 h and then the free convection bridge output voltage, $E(0)$, was measured for gallium temperatures between 328 K and 341 K with no temperature gradient and no magnetic field. A temperature gradient was then applied to the gallium without removing the probe. When the flow reached a steady state, the velocity field was measured. The magnetic field was then applied and when the flow reached a steady state, the velocity field was again measured. After all the velocity data were taken, the hot-film probe was removed from the gallium and replaced by a type T thermocouple. The measurement process was repeated to map the temperature fields under the same conditions used when the velocity field was measured.

Determination of the velocity from the measured anemometer voltage involved first finding the zero velocity anemometer voltage, $E(0)$, for each measurement and then using $E(0)$ and the measured voltage $E(Pe)$ to find $X(Pe)$ and finally using $X(Pe)$ to find the velocity. This process was repeated each time the probe was re-immersed into the molten gallium to account for the change in the impurity layer. The measured $E(0)$—temperature data were then fitted to

$$E(0) = B_0 + B_1 T + B_2 T^2. \tag{6}$$

Typical results are shown in Fig. 5 and typical values for the constants are given in Table 2. The zero velocity voltage decreases as temperature increases because of the smaller probe overheat ratio.

Each anemometer voltage, $E(Pe)$, was converted to $X(Pe)$ using Eq. (4), and the zero velocity voltage, $E(0)$, from Eq. (6). For each $X(Pe)$, a velocity can be found that corresponds to temperatures of 328 K, 333 K, 339 K and 341 K using Eq. (5) and the constants are listed in Table 2.

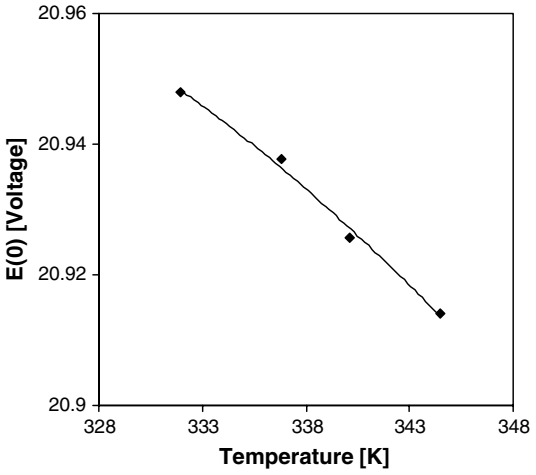

Fig. 5. $E(0)$-temperature curve for the hot-wire velocity probe.

The four velocity–temperature pairs can then be curve-fit to

$$U = C_0 + C_1 T + C_2 T^2. \tag{7}$$

The flow velocity is found by inserting measured temperature T and curve fitting constants C_0, C_1 and C_2 into Eq. (7).

The temperature measurement has a bias uncertainty of ± 0.5 K. The measured velocities have a bias uncertainty of ± 0.5 cm/s.

3. Numerical model

The numerical model used to compare with the experimental measurements in the present study is described in detail by Shu et al. [11] and thus only a brief description of the points pertinent to the present study is given. For molten gallium contained in a rectangular cavity that is subject to a horizontal temperature gradient and a static applied magnetic field (Fig. 1), governing equations are written in a non-dimensionalized form,

$$\nabla \cdot \mathbf{u} = 0, \tag{8}$$

$$\frac{\partial \mathbf{u}}{\partial t} + (\mathbf{u} \cdot \nabla)\mathbf{u} = -\nabla p + \nabla^2 \mathbf{u} - GrT\mathbf{g} + Ha^2[(\mathbf{u} \times \mathbf{B}) \times \mathbf{B}], \tag{9}$$

$$\frac{\partial T}{\partial t} + \mathbf{u} \cdot \nabla T = \frac{1}{Pr} \nabla^2 T, \tag{10}$$

where $\mathbf{u}$ is the velocity vector, T the temperature, p the pressure, t the time, $\mathbf{g}$ the vertical downward unit vector, and $\mathbf{B}$ the applied magnetic field. In the above equations, length is non-dimensionalized using L, velocity using ν/L, time using L^2/ν and temperature using $T_h - T_c$, where L is the distance between the two shaded walls in Fig. 1, ν the kinematic viscosity, T_h and T_c the temperatures at the hot and the cold wall, respectively. The dimensionless numbers governing the flow are Prandtl number (Pr), Grashof number (Gr), and Hartmann number (Ha), which are written as

$$Pr = \frac{v}{\alpha}, \quad Gr = \frac{g\beta(T_h - T_c)L^3}{v^2} \quad \text{and} \quad Ha = BL\sqrt{\frac{\sigma}{\mu}},$$

where α is the thermal diffusivity, g the gravitational acceleration, β the thermal expansion coefficient, the electrical conductivity of the fluid, and μ is the dynamic viscosity. For the molten gallium, the Prandtl number used in calculation is 0.02. The last term on right hand side of Eq. (9) represents the Lorentz force applied by the external magnetic field. For simplified 2-D cases, the governing equations are subject to the following boundary conditions:

$$\mathbf{u} = \mathbf{0} \text{ at } x = 0, \ x = 1 \quad \text{and} \quad y = 0$$

$$\text{and} \quad \frac{\partial \mathbf{u}}{\partial y} = 0 \text{ at } y = 1,$$

$$\frac{\partial T}{\partial y} = 0 \text{ at } y = 0, \ T = 0 \text{ at } x = 1 \quad \text{and}$$

$$T = 1 \text{ at } x = 0,$$

$$\frac{\partial T}{\partial y} = -Bi(T - T_\infty) \quad \text{at } y = 1,$$

where Bi is the Biot number at the top surface, and T_∞ the ambient air temperature. The two vertical walls are kept at constant temperatures and the bottom wall is thermally insulated. At the top surface, flow is free of shear stress and rejects heat to the ambient via convection.

The governing equations along with the boundary conditions are solved using the standard Galerkin finite element method. Details of model development and mesh independence study were given in [11]. In the present study, 900 4-node elements with 31 nodes in both X and Y directions are used. The node spacing decreases from the center toward the walls following an arithmetic progressive ratio of 0.2. The non-uniform mesh ensures denser grid near the solid walls. This mesh arrangement is adequate for the present studies and any further mesh refinement produces results with an error less than 0.5%.

4. Results and discussion

The hot water in the thermal baths on either side of the container holding the gallium was adjusted until the temperatures at the inside center of the coppers plates reached

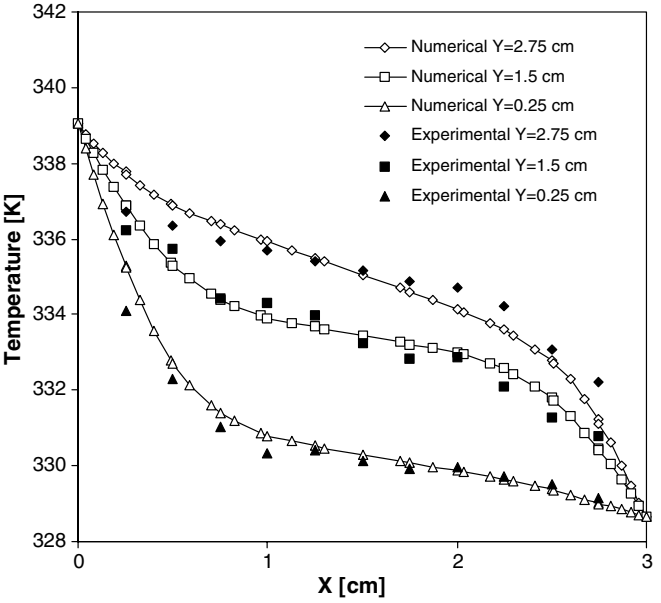

Fig. 7. Comparison of the experimentally measured and numerically calculated temperature distributions across the cell at different vertical locations, subject to an externally applied magnetic field of 300 Gauss.

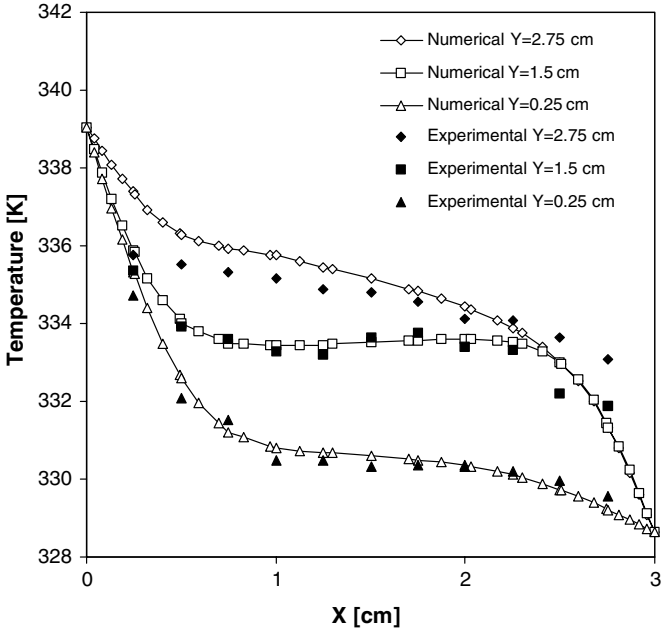

Fig. 6. Comparison of the experimentally measured and numerically calculated temperature distributions across the cell at different vertical locations without externally applied magnetic field.

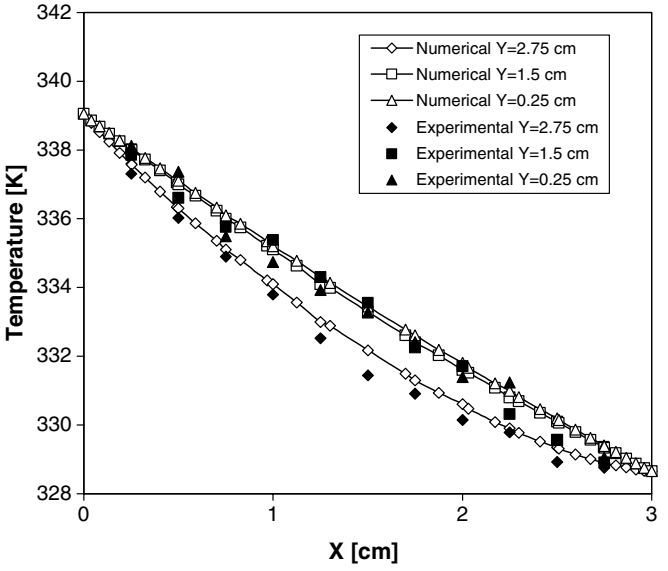

Fig. 8. Comparison of the experimentally measured and numerically calculated temperature distributions across the cell at different vertical locations, subject to an externally applied magnetic field of 3500 Gauss.

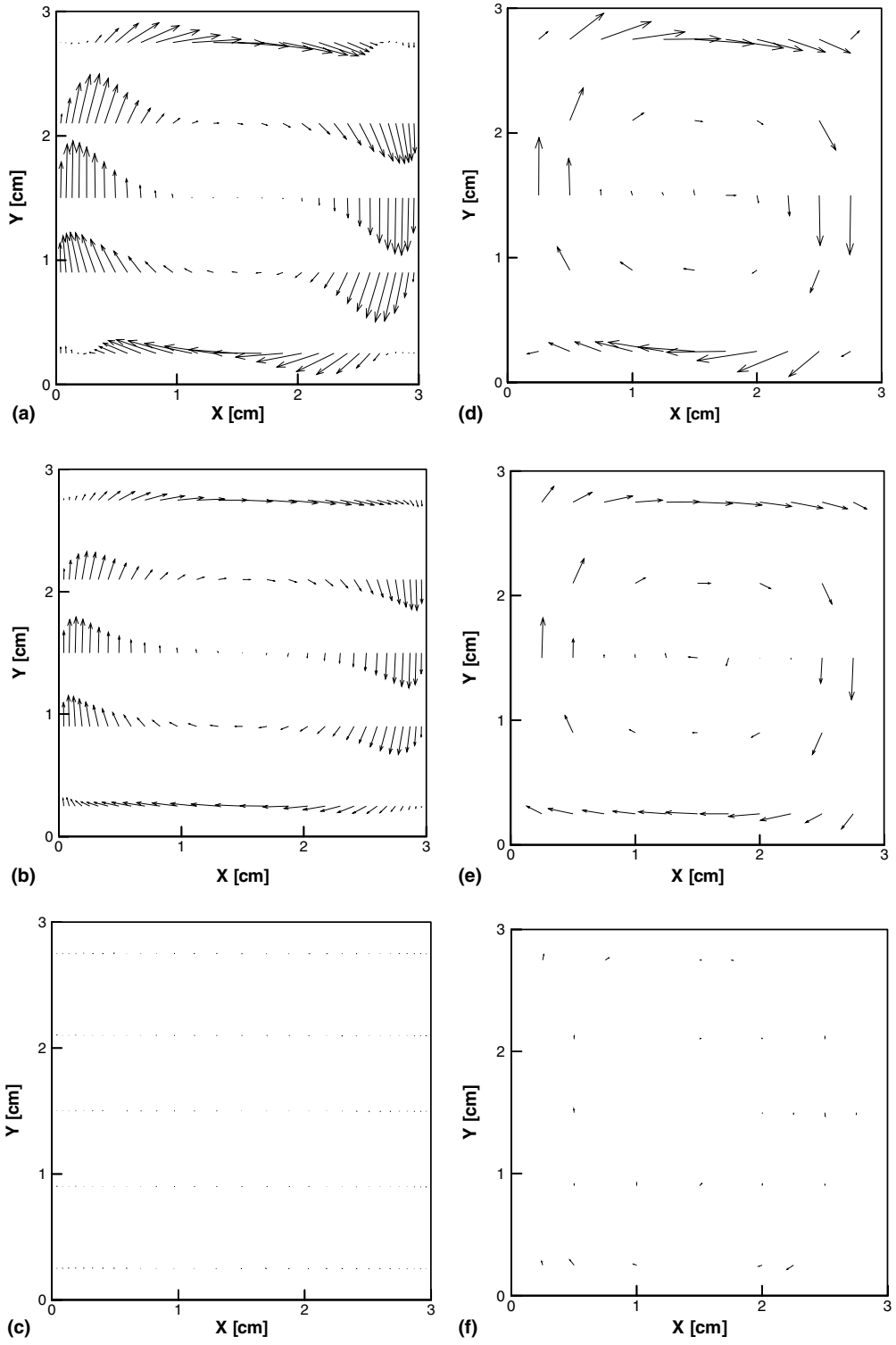

Fig. 9. Comparison of computed and measured vector velocity distribution in the molten gallium for various field strengths: (a–c) Numerical results without magnetic field (a), with the field strength of 300 Gauss (b) and with the field strength of 35 Gauss; and (d–f) measured velocity field without magnetic field (d), with the field strength of 300 Gauss and (c) with the field strength of 3500 Gauss.

328 K and 339 K, giving a $\Delta T = 11$ K. All experimental measurements were made for this temperature difference. During the experiments the room air was fairly constant at 293 K.

The measured and computed temperature profiles with applied magnetic fields of 0 Gauss, 300 Gauss, and 3500 Gauss are shown in Figs. 6–8, respectively. In each of the figures, the temperature profiles across the width

of the cell are plotted for $Y = 2.75$ cm, 1.5 cm and 0.25 cm. The non-linear temperature distributions depicted in Fig. 6 are clearly a manifestation of the strong natural convection present in the testing cell. The temperature profiles along the X direction become less-distorted with an imposed magnetic field of 300 Gauss, suggesting that the applied field helps to reduce the convection. This magnetic damping effect is evident in Fig. 7. When the applied magnetic field reaches 3500 Gauss, the temperature profile is nearly linear, indicating that the convective flow is substantially reduced, and the primary heat transfer mechanism between the hot and cold walls is by conduction, as appears in Fig. 8. It is noted that in an idealized natural convection cell with the top and bottom thermally insulated perfectly, the temperature distributions at equal distance above and below the centerline ($Y = 1.5$ cm) exhibit certain symmetry structure [11]. Such a symmetry, however, is not observed between the experimental measured temperature profiles at $Y = 2.75$ cm and $Y = 0.25$ cm. This asymmetric profile is apparently caused by the heat loss from the top surface of the gallium to the surrounding cooler air, which decreases the temperature near the top surface at $Y = 2.75$ cm. The heat loss at the top surface, however, has little effect on the temperature profiles at $Y = 1.5$ cm and 0.25 cm. Similar asymmetry was also reported by Juel et al. [32]. With the presence of the magnetic fields, the convective flow becomes weaker, thereby resulting in less heat being lost at the top surface and the thermal profiles becoming closer in symmetry to the idealized system. For the present system, even with a moderate magnetic field strength of 300 Gauss, an obvious temperature drop is observed along $Y = 2.75$ cm, as appears in Fig. 7, which indicates that the 300 Gauss magnetic field is not strong enough to suppress the natural convection.

As a comparison, numerical predictions are also plotted along with the measurements in Figs. 6–8. The computed temperature profiles at $Y = 0.25$ and 1.5 cm are in good agreement with the experimental data, but less satisfactory at $Y = 2.75$ cm for the case without an applied magnetic field. For all the cases, the measured temperature profiles agree with the numerical simulations better along the center-line of the testing cell. It should be noted that various heat transfer coefficients at the top surface were tested to match the temperature profile at $Y = 2.75$ cm. The numerical simulations show that for this system the heat loss at the top surface does not have a strong effect on the calculated bulk flow velocity profile.

The velocity vector maps from the experimental measurements and numerical simulations are depicted in Fig. 9 for three different magnetic fields applied. The scale factor used for the plot is approximately 1.8 cm/s per cm. The direction of the measured velocities are determined by the numerical predictions, as the hot-wire probes measure only the magnitude of the velocity. For a very small velocity, measurement uncertainties sometimes generate a non-physical negative velocity magnitude, which was set to zero. Examination of the results in Fig. 9 illustrates that an anti-clockwise convection cell is developed in the system as a result of an imposed thermal gradient and the fluid moves downward near the cold wall and upward near the hot wall. This recirculating flow structure is shown in both predictions and measurements. Note also that the velocity magnitudes match very well both qualitatively and quantitatively between the predicted and measured data. Both the numerical simulations and experimental measurements indicate that the velocity is suppressed with an imposed magnetic field and the reduction in velocity is more significant with an increase in applied magnetic fields. With the field strength of 3500 Gauss, the velocity field is reduced essentially beyond detection by the hot-film probe.

To further quantify the magnetic damping effects, the measured velocity magnitude distributions across the cell along $Y = 2.75$ cm, 1.5 cm and 0.25 cm are illustrated in Figs. 10–12, respectively. Each figure gives the profiles for the three levels of the applied magnetic field strength. In light of the vector velocity fields plotted in Fig. 9, it is clear that the flows are parallel to the top and bottom walls, but in the opposite directions, with the maximum at the middle ($X = 1.5$ cm) for $Y = 2.75$ cm (Fig. 10) and $Y = 0.25$ cm (Fig. 12). The maximum of the measured velocity (in magnitude) distribution across the cell at $Y = 1.5$ cm occurs near the two sidewalls, where the flow moves upward and downward along the walls. Inspection of the results in Figs. 10–12 indicates that the measured velocity decreases when the applied magnetic field is increased. With a moderate magnetic field strength of 300 Gauss, the maximum velocity is reduced to about 60% of that without the magnetic field. As the magnetic field strength increases to 3500 Gauss, the velocity is suppressed to nearly zero within the experimental uncertainty. This supports the measured near-linear temperature profile at 3500 Gauss shown in Fig. 8. For the purpose of comparison, Figs. 10–12 also

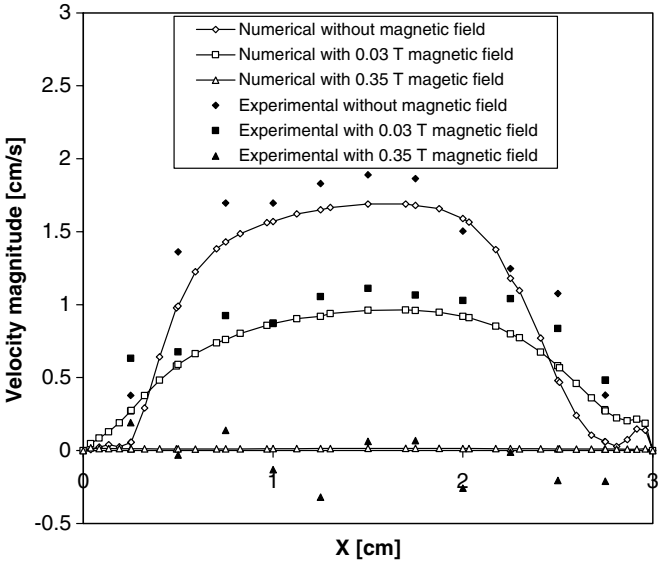

Fig. 10. Dependence of velocity (in magnitude) distribution upon an applied magnetic field along $Y = 2.75$ cm.

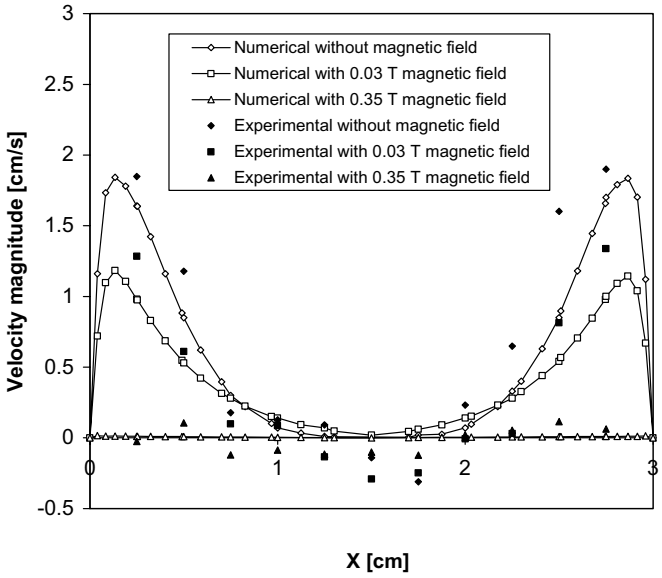

Fig. 11. Dependence of velocity (in magnitude) distribution upon an applied magnetic field along $Y = 1.5$ cm.

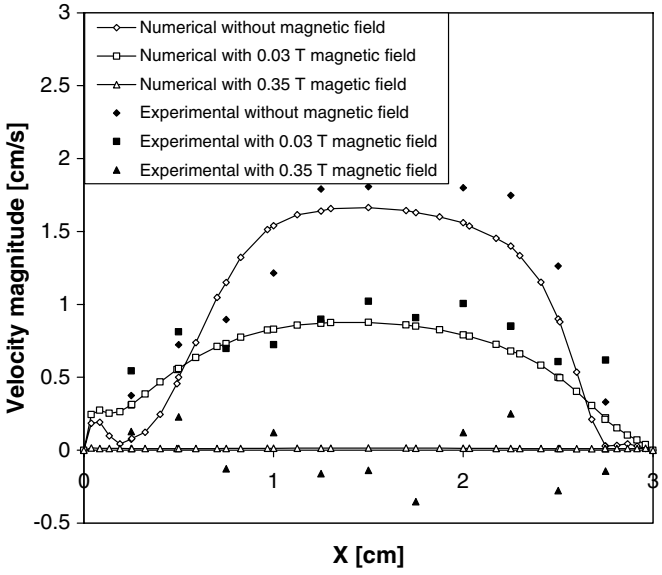

Fig. 12. Dependence of velocity (in magnitude) distribution upon an applied magnetic field along $Y = 0.25$ cm.

show the velocity magnitudes obtained from numerical computations. The computations agree well with the experimental measurements within the experimental uncertainty of 0.5 cm/s.

It could be remarked here that the flow sensed by the hot-film probe is a combination of natural convection induced by the probe and the main natural convective flow due to the temperature gradient across the cell. Therefore the measured velocity profiles agree with the numerical simulations better at higher velocity magnitudes, near $X = 15$ cm in Figs. 10 and 12 and near the sidewalls in Fig. 11.

5. Concluding remarks

This paper presents an experimental investigation of natural convection driven by a temperature gradient in a molten metal contained in a rectangular enclosure with and without the presence of an external magnetic field. Liquid gallium was used as a working fluid. Both the temperature and velocity fields were measured. The temperature profile was determined using a thermocouple and the melt flow velocity was measured using a standard constant temperature hot-film anemometer. The hot-film probe was calibrated in a rotating container filled with molten gallium. The calibration is carried out over the expected velocity range at a series of discrete constant temperatures over the expected temperature range to compensate the temperature gradient. The probes, so calibrated, are then used to measure the natural convection field. The measured velocity field exhibits a recirculating cell, which is consistent with numerical predictions obtained from a numerical model reported in an early study. The flow structure remains the same with and without an applied magnetic field. The magnitude of the velocity, however, is reduced with an increase in applied magnetic field strengths. The reduction in convection is also manifested in the measured thermal profiles, which approach to a linear distribution across the cell as the magnetic field increases in strength. The measured velocity and temperature profiles compare reasonably well with the numerical predictions.

Acknowledgements

The authors acknowledge the financial support of this work by NASA (Grant No. NAG8-1693) and the assistance provided by Mr. Robert Lentz.

References

[1] W.E. Langlois, Buoyancy-driven flows in crystal-growth melts, Ann. Rev. Fluid Mech. 17 (1985) 191–215.
[2] J.S. Walker, The role of magnetic fields in crystal growth, in: K.W. Benz (Ed.), Process in Crystal Growth and Characterization of Materials, vol. 38, Elsevier, Amsterdam, 1999, pp. 195–213.
[3] C.W. Lan, Recent progress of crystal growth modeling and growth control, Chem. Eng. Sci. 59 (2004) 1437–1457.
[4] H. Ozoe, K. Okada, The effect of the direction of the external magnetic field on the three-dimensional natural convection in a cubic enclosure, Int. J. Heat Mass Transfer 32 (1989) 1939–1953.
[5] T. Alboussière, J.P. Garandet, R. Moreau, Asymptotic analysis and symmetry in MHD convection, Phys. Fluids 8 (1996) 2215–2226.
[6] H. BenHadid, D. Henry, Numerical study of convection in the horizontal Bridgman configuration under the action of a constant magnetic field. Part 2. Three-dimensional flow, J. Fluid Mech. 333 (1997) 57–83.
[7] J.P. Garandet, T. Alboussière, R. Moreau, Buoyancy-driven convection in a rectangular enclosure with a transverse magnetic field, Int. J. Heat Mass Transfer 35 (1992) 741–748.
[8] J. Baumgartl, G. Müller, The use of magnetic fields for damping the action of gravity fluctuations (g-jitter) during crystal growth under microgravity, J. Cryst. Growth 169 (1996) 582–586.

[9] N. Ma, J.S. Walker, Magnetic damping of buoyant convection during semiconductor crystal growth in microgravity. Continuous random g-jitters, Phys. Fluids 8 (4) (1996) 944–949.
[10] B. Pan, D.-Y. Shang, B.Q. Li, H.C. de Groh, Magnetic field effects on g-jitter induced flow and solute transport, Int. J. Heat Mass Transfer 45 (2002) 125–144.
[11] Y. Shu, B.Q. Li, H.C. de Groh III, Magnetic damping of g-jitter induced double-diffusion convection, Num. Heat Transfer, Part A 42 (2002) 345–364.
[12] D.T.J. Hurle, Temperature oscillations in molten metals and their relationship to growth striae in melt-grown crystals, Philos. Mag. 13 (1966) 305–310.
[13] D.T.J. Hurle, E. Jakeman, C.P. Johnson, Convective temperature oscillation in molten gallium, J. Fluid Mech. 64 (1974) 565–576.
[14] K. Okada, H. Ozoe, Experimental heat transfer rate of natural convection of molten gallium suppressed under an external magnetic field in either *X*, *Y*, or *Z* direction, J. Heat Transfer 114 (1992) 107–114.
[15] L. Davoust, M.D. Cowley, R. Moreau, R. Bolcato, Buoyancy-driven convection with a uniform magnetic field. Part 2. Experimental investigation, J. Fluid Mech. 400 (1999) 59–90.
[16] T. Alboussière, J.P. Garandet, R. Moreau, Buoyancy-driven convection with a uniform magnetic field. Part 1. Asymptotic analysis, J. Fluid Mech. 253 (1993) 545–563.
[17] H. BenHadid, D. Henry, Numerical simulation of convective three-dimensional flows in a horizontal cylinder under the action of a constant magnetic field, J. Cryst. Growth 166 (1996) 436–445.
[18] A. Juel, T. Mullin, H. BenHadid, D. Henry, Magnetohydrodynamic convection in molten gallium, J. Fluid Mech. 378 (1999) 97–118.
[19] B. Hof, A. Juel, T. Mullin, Magnetohydrodynamic damping of convective flows in molten gallium, J. Fluid Mech. 482 (2003) 163–179.
[20] D. Brito, P. Cardin, H.-C. Nataf, G. Marolleau, Experimental study of a geostrophic vortex of gallium in a transverse magnetic field, Phys. Earth Planet. Interiors 91 (1995) 77–98.
[21] J.M. Aurnou, P.L. Olson, Experiments on Rayleigh–Bénard convection, magnetoconvection and rotating magnetoconvection in liquid gallium, J. Fluid Mech. 430 (2001) 283–307.
[22] M. Sajben, Hot wire anemometer in liquid metal, Rev. Sci. Instrum. 36 (1965) 945–949.
[23] D.G. Malcolm, Some aspects of turbulence measurement in liquid mercury using cylindrical quartz-insulated hot-film sensors, J. Fluid Mech. 37 (1969) 701–713.
[24] C.B. Reed, B.F. Picologlou, P.V. Dauzvardis, J.L. Bailey, Techniques for measurement of velocity in liquid-metal MHD flow, Fusion Technol. 10 (1986) 813–821.
[25] H.H. Bruun, Hot-film Anemometry: Principles and Signal Analysis, Oxford University Press, Oxford, 1995.
[26] C.G. Lomas, Fundamentals of Hot Wire Anemometry, Cambridge University Press, Cambridge, UK, 1986.
[27] D.G. Malcolm, Magnetohydrodynamic effect on hot-film measurements in mercury, DISA Info. 9 (1970) 27–29.
[28] R.J. Holroyd, Hot-film probe velocity measurements in liquid metal MHD duct flow experiments, DISA Info. 25 (1980) 19–24.
[29] P.S. Lykoudis, P.F. Dunn, Magneto-fluid-mechanics heat transfer from hot-film probes, Int. J. Heat Mass Transfer 16 (1973) 1439–1452.
[30] D.C. Collis, M.J. Williams, Two-dimensional convection from heated wire at low Reynolds numbers, J. Fluid Mech. 6 (1959) 357–384.
[31] C. Trakas, P. Tabeling, J.P. Chabrerie, Low-velocity calibration of hot-film sensors in mercury, J. Phys. E: Sci. Instrum. 16 (1983) 568–570.
[32] A. Juel, T. Mullin, H. BenHadid, D. Henry, Three-dimensional free convection in molten gallium, J. Fluid Mech. 436 (2001) 267–281.